An Open Source Dual Purpose Acrobot and Pendubot Platform for Benchmarking Control Algorithms for Underactuated Robotics

Felix Wiebe[1], Shivesh Kumar[1,2], Lasse J. Shala[1], Shubham Vyas[1], Mahdi Javadi[1], Frank Kirchner[1,3]

I. Introduction

Motivation

Recent interest in the control of underactuated robots has surged significantly due to the impressive athletic behaviors shown by robots developed by e.g. Boston Dynamics[4], Agility Robotics[5] and MIT [1]. This gives rise to the need for canonical robotic hardware setups for studying underactuation and comparing learning and control algorithms for their performance and robustness. Similar to OpenAIGym [2] and Stable Baselines [3] which provide simulated benchmarking environments and baselines for reinforcement learning algorithms, there is a need for benchmarking learning and control methods on real canonical hardware setups. To encourage reproducibility in robotics and artificial intelligence research, these hardware setups should be affordable, easy to manufacture with off-the-shelf components and the accompanying software should be open-source. Acrobot and pendubot are classical textbook examples for canonical underactuated systems with strong non-linear dynamics and their swing-up and upright balancing is considered a challenging control problem, especially on real hardware.

This paper presents an open-source and low-cost test bench for validating, comparing and benchmarking the performance of control algorithms for underactuated robots with strong non-linear dynamics. It introduces a double pendulum platform built using two off-the-shelf quasi-direct drives (QDDs). Due to low friction and high mechanical transparency offered by QDDs, one of the actuators can be kept passive and be used as an encoder, so that the system can be operated as a double pendulum, a pendubot or an acrobot without changing the hardware. Using the proposed platform, trajectory optimization and control algorithms for the swing-up and upright stabilization of the acrobot and pendubot systems are compared and benchmarked. We show that, by considering simple variations of the design, the difficulty of the control problem can be varied giving researchers opportunity for showing the robustness of their control algorithms. We demonstrate the transfer of one examplary controller from the simulation to the real hardware with successful swing-ups on pendubot and acrobot.

This work has been performed in the M-RoCK project funded by the German Aerospace Center (DLR) with federal funds (Grant Number: FKZ 01IW21002) from the Federal Ministry of Education and Research (BMBF) and is additionally supported with project funds from the federal state of Bremen for setting up the Underactuated Robotics Lab (Grant Number: 201-342-04-2/2021-4-1). Author 4 acknowledges support from the Stardust Reloaded project which has received funding from the European Union's Horizon 2020 research and innovation programme under the Marie Skłodowska-Curie grant agreement No 813644.

[1]Robotics Innovation Center, DFKI GmbH, Bremen, Germany firstname.lastname@dfki.de

[2]Division of Dynamics, Department of Mechanics & Maritime Sciences, Chalmers University of Technology, Gothenburg, Sweden.

[3]AG Robotics, Department of Mathematics and Computer Science, University of Bremen, Germany frank.kirchner@uni-bremen.de

[4]https://www.bostondynamics.com

[5]https://agilityrobotics.com/robots

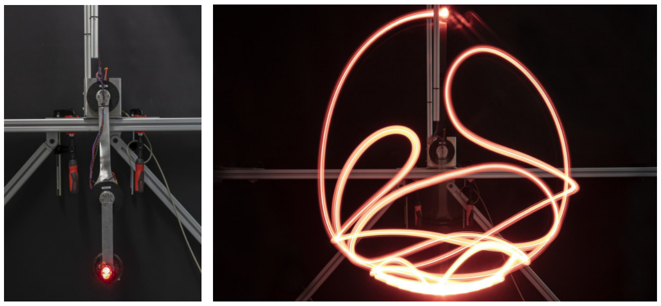

(a) Hardware (b) Freefall

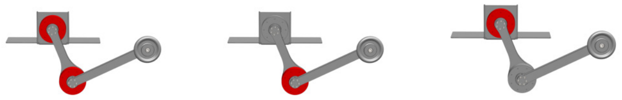

(c) Double Pendulum (d) Acrobot (e) Pendubot

Fig. 1: Double pendulum test bench. (a) shows the hardware setup, (b) shows a long exposure shot of the free falling double pendulum, (c)-(e) illustrate how the usage as a fully actuated double pendulum, an acrobot or a pendubot by selectively activating only the needed motor(s) (colored in red).

Related Work

Acrobot is an underactuated robotic system inspired by a *Gymnastic Acrobat* and was first introduced in [4]. Following this, a large body of research on the dynamics and control of such systems was carried out. However, over the years, the work carried out experimentally has been few and far in between in comparison to the theoretical work demonstrated only in simulation. The earliest work on balancing an experimental acrobot at the top-most position and other unstable equilibrium points can be seen in [5] where a (single input) pseudolinearizing controller was used for the balancing task. Along with this, a region of attraction (RoA) analysis was performed for the given controller. The initial problem of *swing-up and balance* for the acrobot was formulated and demonstrated on a real system in [6] where partial feedback linearization and energy-based control was used to perform the swing-up while linear quadratic regulation (LQR) was used to balance at the top. A first comparative study on the balancing controllers was carried out in [7] with both theoretical RoA analysis and experimental validation along with introducing an additional balancing controller. Following this, an energy-based swing-up designed using Lyapunov stability theory with LQR for top stabilization was showcased in experiments in [8]. In recent works, Sums-of-Squares based methods have been used to synthesize robust controllers for swing-up trajectory tracking and top-balancing [9]. Furthermore, online-trajectory planning for the swing-up and balance task using model predictive control with particle swarm optimization was demonstrated on a physical system in [10]. Recently for the first time, both swing-up and balancing were achieved with a single controller using the stable manifold approach [11]. It is interesting to note that all experimental implementations of the acrobot mount the actuator at the base link and a transmission is used for actuating the second joint in order to minimize moving inertia. For the Pendubot system, which in contrast to the Acrobot, has the first joint actuated, a larger body of research can be found for experimental results (e.g. [12], [13]). Due to mechanical design and control complexity, all reported platforms in the literature were constructed for a single purpose, either the Pendubot or the Acrobot. Only a recent parallel development showed a system that could potentially be used as a testbed for both Pendubot and Acrobot [14]. The system is provided with open source MATLAB code. However, the system is complex to construct due to the use of belt transmissions and the provided software requires a MATLAB license which increases the accessibility barrier. Until now, a fully open-source test platform for acrobot/pendubot type system with direct joint actuation is not available.

II. Mechatronics System Design

This section presents the mechatronic system design of the dual purpose acrobot-pendubot hardware.

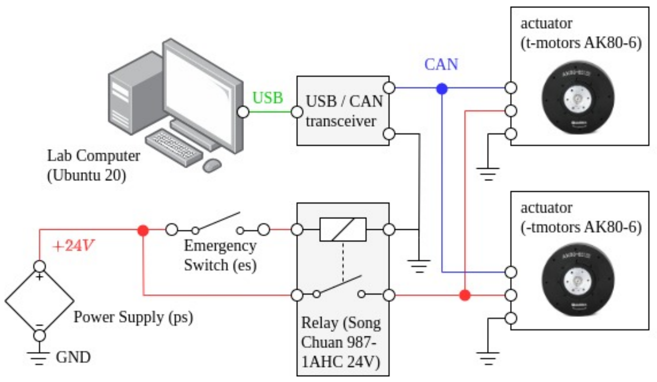

Fig. 2: Mechatronic system design of dual purpose double pendulum.

A. Mechanical Design

The mechanical design (see Fig. 1) consists of a shoulder motor mounting bracket made of folded aluminum, and two light-weight links which are made of laser cut 1 mm thick sandwich aluminum plates with a laminate of 15 mm PVC rigid foam board (Airex) in between. By using sandwich materials, the weight of the pendulum arms can be kept very low in relation to the drives and the end effector weight. The end of the first link contains the elbow motor housing and the end of second link mounts the weight of $0.5\,\mathrm{kg}$. Two variations of both links ($0.2\,\mathrm{m}$ and $0.3\,\mathrm{m}$ long) are manufactured which allows changing the complexity of the control problem. Since, the used motors do not provide a hollow shaft, a cabling guide is mounted to the first link in the opposite direction to prevent windup of cables.

B. Electronics & Processing Architecture

Both shoulder and elbow actuators consist of off-the-shelf AK80-6 QDDs from T-Motors[6] with a gear ratio of 6:1, maximum speed of $38.22\,\mathrm{rad\,s^{-1}}$, maximum continuous torque of $6\,\mathrm{N\,m}$ and peak torque of $12\,\mathrm{N\,m}$. The low friction offered by these motors enable chaotic dynamics in the system which is interesting for control purposes (see Fig. 1(b) for its freefall). The two motors communicate with a standard Intel Core-i7 PC via a CAN-USB/2 interface from ESD. The setup allows a real-time position, velocity and torque control with a control frequency of 1 kHz with Python on a standard PC. The power supply used is EA-PS 9032-40 from Elektro-Automatik which can provide a maximum voltage of $36\,\mathrm{V}$ and $48\,\mathrm{A}$ current. A capacitor bank of ten single $2.7\,\mathrm{V}/400\,\mathrm{F}$ capacitor cells connected in series resulting a total capacity of $40\,\mathrm{F}$ is wired in parallel to the motor to protect the power supply from back EMF. An emergency stop button which disconnects the actuator from the power supply and capacitor is also integrated as an additional safety measure. A schematic of the electronial setup can be found in Fig. 2.

III. Methodology

This section gives an overview over the mathematical modeling of the double pendulum, the identification of the dynamic parameters, as well as the methods used for controlling the double pendulum as acrobot and pendubot.

A. Dynamics

We model the dynamics of the double pendulum with 15 parameters which include 8 link parameters namely masses (m_1, m_2), lengths (l_1, l_2), center of masses (r_1, r_2), inertias (I_1, I_2) for the two links, and 6 actuator parameters namely motor inertia (I_r), gear ratio g_r, coulomb friction (c_{f1}, c_{f2}), viscous friction (b_1, b_2) for the two joints[7] and gravity (g). The generalized coordinates $\boldsymbol{q} = (q_1, q_2)^T$ are the joint angles measured from the free hanging position. The state

[6]https://store.tmotor.com/goods.php?id=981

[7]We found that the friction parameters for two actuators of the same type can be different due to manufacturing differences.

vector of the system contains the coordinates and their time derivatives: $\boldsymbol{x} = (\boldsymbol{q}, \dot{\boldsymbol{q}})^T$. The torques applied by the actuators are $\boldsymbol{u} = (u_1, u_2)$. The equations of motion of a dynamical system can be written as

$$\dot{\boldsymbol{x}} = \boldsymbol{f}(\boldsymbol{x}, \boldsymbol{u}) \tag{1}$$

$$= \begin{bmatrix} \dot{\boldsymbol{q}} \\ \boldsymbol{M}^{-1}(\boldsymbol{q})(\boldsymbol{D}\boldsymbol{u} - \boldsymbol{C}(\boldsymbol{q}, \dot{\boldsymbol{q}})\dot{\boldsymbol{q}} + \boldsymbol{G}(\boldsymbol{q}) - \boldsymbol{F}(\dot{\boldsymbol{q}})) \end{bmatrix} \tag{2}$$

The dynamic matrices $\boldsymbol{M}, \boldsymbol{C}, \boldsymbol{G}, \boldsymbol{F}$ and $\boldsymbol{D}$ that we used to describe our double pendulum test bench can be found in the supplementary material.

B. System Identification

For the identification of the 15 model parameters, we fix the natural, provided and easily measurable parameters g, g_r, l_1 and l_2. The equations of motion are then linear in the following (composed) model parameters:

$$m_1 r_1,\ m_2 r_2,\ m_2,\ I_1,\ I_2,\ I_r,\ b_1,\ b_2,\ c_{f1},\ c_{f2}. \tag{3}$$

By executing excitation trajectories on the real hardware, data tuples of the form $(\boldsymbol{q}, \dot{\boldsymbol{q}}, \ddot{\boldsymbol{q}}, \boldsymbol{u})$ can be recorded. For finding the best system parameters, one can make use of the fact that the dynamic matrices $\boldsymbol{M}, \boldsymbol{C}, \boldsymbol{G}$ and $\boldsymbol{F}$ are linear in the parameters in (3) and perform a least squares optimization for the equations of motion on the recorded data.

C. Balancing with LQR

The linear quadratic regulator (LQR) controller is a well established and widespread optimal controller which acts on a linear system $\dot{\boldsymbol{x}} = \boldsymbol{A}\boldsymbol{x} + \boldsymbol{B}\boldsymbol{u}$ and an objective which is specified by a quadratic, instantaneous cost function $J = \boldsymbol{x}^T\boldsymbol{Q}\boldsymbol{x} + \boldsymbol{u}^T\boldsymbol{R}\boldsymbol{u}$ with the symmetric and positive definite matrices $\boldsymbol{Q} = \boldsymbol{Q}^T \succeq 0$ and $\boldsymbol{R} = \boldsymbol{R}^T \succ 0$. This allows for reducing the Hamilton-Jacobi-Bellman equation to the algebraic Riccati equation for which good numerical solvers exist. Its solution is the optimal cost-to-go matrix $\boldsymbol{S}$, from which the optimal policy can be inferred:

$$\boldsymbol{u}(\boldsymbol{x}) = -\boldsymbol{R}^{-1}\boldsymbol{B}^T\boldsymbol{S}\boldsymbol{x} = -\boldsymbol{K}\boldsymbol{x}. \tag{4}$$

In order to use an LQR controller for stabilizing the double pendulum on the top, the dynamics have to be linearized around the top position $\boldsymbol{x}^d = [\pi, 0, 0, 0]$ and $\boldsymbol{u}^d = [0, 0]$, and the state and actuation have to be expressed in relative coordinates $\tilde{\boldsymbol{x}} = \boldsymbol{x} - \boldsymbol{x}^d$, $\tilde{\boldsymbol{u}} = \boldsymbol{u} - \boldsymbol{u}^d$.

For the double pendulum with LQR control x^d represents a stable fixpoint and the region of attraction (RoA) $\mathcal{B}$ around that fixpoint describes the set of initial states for which $\boldsymbol{x} \to \boldsymbol{x}^d$ as $t \to \infty$. Direct computation of this set is often not possible. However, it can be estimated by considering the sublevel set of a Lyapunov function $V(\boldsymbol{x})$. When using LQR to stabilize the system around $\boldsymbol{x}^\star$, the cost-to-go can serve as a quadratic Lyapunov function. In this case, the estimated RoA can be written as: $\mathcal{B}_{\text{est}} = \{\boldsymbol{x} | \boldsymbol{x}^T\boldsymbol{S}\boldsymbol{x} \le \rho\}$, where ρ is a scalar that can be estimated using either probabilistic or optimization based methods.

D. Trajectory Optimization with iLQR

Iterative LQR (iLQR) [15] is an extension of LQR to non-linear dynamics. The LQR uses the fixed point linearised dynamics for the entire state space and hence is only useful as long as the linearization error is small. In contrast to LQR, iLQR linearises the dynamics for every given state at each time step and can deal with nonlinear dynamics at the cost of being only able to optimize over a finite time horizon.

As a trajectory optimization method, iLQR solves the following optimization problem:

$$\min_{\boldsymbol{u}_0, \boldsymbol{u}_1, \ldots, \boldsymbol{u}_{N-1}} \boldsymbol{x}_N^T\boldsymbol{Q}_f\boldsymbol{x}_N + \sum_{i=0}^{N-1} (\boldsymbol{x}_i^T\boldsymbol{Q}\boldsymbol{x}_i + \boldsymbol{u}_i^T\boldsymbol{R}\boldsymbol{u}_i) \tag{5}$$
$$\text{subject to :} \qquad \boldsymbol{x}_{i+1} = f_{discrete}(\boldsymbol{x}_i, \boldsymbol{u}_i)$$

where a start state $\boldsymbol{x}_0$ is set beforehand. $\boldsymbol{Q}_f$, $\boldsymbol{Q}$ and $\boldsymbol{R}$ are cost matrices penalizing the final state, intermediate states and the control input respectively. $f_{discrete}$ is the discretization of the system dynamics in (1). Again, $\boldsymbol{x}$ and $\boldsymbol{u}$ can also be expressed in relative coordinates $\tilde{\boldsymbol{x}}$, $\tilde{\boldsymbol{u}}$.

E. Trajectory Stabilization Controllers

1) TVLQR: Time-Varying LQR (TVLQR) is another extension to the regular LQR algorithm and can be used to stabilize a nominal trajectory $(\boldsymbol{x}^d(t), \boldsymbol{u}^d(t))$. For this, the LQR formalization is used for time-varying linear dynamics

$$\dot{\boldsymbol{x}} = \boldsymbol{A}(t)(\boldsymbol{x} - \boldsymbol{x}^d(t)) + \boldsymbol{B}(t)(\boldsymbol{u} - \boldsymbol{u}^d(t)) \tag{6}$$

which requires to linearise (1) at all steps around $(\boldsymbol{x}^d(t), \boldsymbol{u}^d(t))$. This results in the optimal policy at time t

$$\boldsymbol{u}(\boldsymbol{x}, t) = \boldsymbol{u}^d - \boldsymbol{K}(t)(\boldsymbol{x} - \boldsymbol{x}^d(t)). \tag{7}$$

2) iLQR with Riccati Gains: During the iLQR optimization process the trajectory is altered with Riccati gain matrices. During the execution these Riccati gains can be used to stabilize the trajectory as discussed in [16].

3) iLQR MPC Stabilization: iLQR is a shooting method and as such has the property that all trajectories during the optimization process are physically feasible. So even when stopped before convergence, the solution is not inconsistent. This has the advantage that iLQR can be used in a Model Predictive Control (MPC) ansatz. For this the optimization is performed online and at every time step the first control input $\boldsymbol{u}_0$ is executed. For the next time step the previous solution is used to warm start the next optimization step. For stabilizing a nominal trajectory, the iLQR optimization problem (5) is solved with time varying desired states $\boldsymbol{x}^d = \boldsymbol{x}^d(t)$ and inputs $\boldsymbol{u}^d = \boldsymbol{u}^d(t)$.

F. Policy-based Controllers

1) iLQR MPC (free): The iLQR MPC method can also solve the full optimization problem online without a nominal trajectory. For this the optimization problem is solved with a fixed goal state $\boldsymbol{x}^d$.

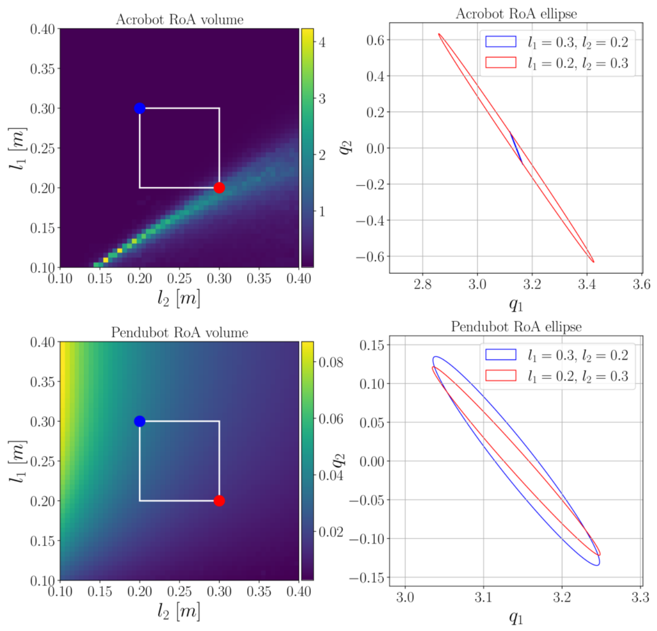

Fig. 3: RoA volume as a function of design parameters l_1 and l_2 (left) and associated RoA projections of two design variations $\mathcal{D}_1$ (blue) and $\mathcal{D}_2$ (red) (right).

2) *Partial Feedback Linearization:* Partial Feedback Linearization (PFL) [6] is a classical method from control theory. With PFL it is possible to provoke a linear response in both joints of the double pendulum even if operated as a pendubot or acrobot. For an intuition of its functionality consider the lower part of (2) for the acrobot ($u_1 \equiv 0$). The unactuated upper part of the vector equation can be solved for the acceleration $\ddot{q}_1$ and then plugged into the lower part of the equation. The control input u_2 can now be designed as PD control with an energy term

$$u_2(\boldsymbol{x}) = -k_p(q_2 - q_2^d) - k_d\dot{q}_2 + k_e(E - E^d)\dot{q}_1 \quad (8)$$

with the desired configuration q_2^d of the second link, the total energy E, the desired total energy E^d and the gain parameters k_p, k_d and k_e. The above described method is called collocated PFL. Similarly, it is also possible to eliminate $\ddot{q}_2$ instead of $\ddot{q}_1$ from the equations which is than called non-collocated PFL. Partial feedback linearization for the pendubot can be done in the same way. The collocated control law in this case reads

$$u_1(\boldsymbol{x}) = -k_p(q_1 - q_1^d) - k_d\dot{q}_1 + k_e(E - E^d)\dot{q}_2. \quad (9)$$

IV. Controller Comparison

This section explains how the design parameters were chosen, states the results from the dynamic system identification, introduces the controller robustness criteria and presents the results of the controller comparison.

A. System Design

Our double pendulum setup allows to use different link lengths l_1 and l_2. Under the assumption, that acrobot and pendubot each benefit of different ratios of link lengths, we aimed to find two designs, one tailored to the acrobot and the other to the pendubot configuration. In the following, we consider the closed loop dynamics of the system under LQR control and focus on the volume of the RoA associated to the fixed point of the upright pose. Link lengths l_1 and l_2 have been determined by employing a design optimization similar to the one introduced in [17] with the only difference, that the RoA estimation was carried out using Sums-of-Squares (SOS) optimization.

During the optimization, the masses were kept constant ($m_1 = m_2 = 0.6\,\mathrm{m}$) and we assumed point masses ($r_1 = l_1, r_2 = l_2, I_1 = m_1 l_1^2, I_2 = m_2 l_2^2$). The LQR control weights, the $\boldsymbol{Q}$ and $\boldsymbol{R}$ matrices, were set to unit matrices. We searched for lengths between $0.2\,\mathrm{m}$ and $0.3\,\mathrm{m}$ to ensure that we can actually construct and operate the hardware.

The optimizations resulted in two designs $\mathcal{D}_1$ and $\mathcal{D}_2$. Design $\mathcal{D}_1$ was optimized for the pendubot and features a longer first link ($l_1 = 0.3\,\mathrm{m}, l_2 = 0.2\,\mathrm{m}$), while $\mathcal{D}_2$ was optimized for the acrobot and has switched link lengths ($l_1 = 0.2\,\mathrm{m}, l_2 = 0.3\,\mathrm{m}$). The left-hand side of Fig. 3 shows the volume of $\mathcal{B}_{\text{est}}$ for acrobot (top) and pendubot (bottom) as a function of the design variables l_1 and l_2. The right-hand side shows slices of the estimated RoA of each model in the q_1 vs. q_2 plane (for $\dot{q}_1 = \dot{q}_2 = 0$) for acrobot (top) and pendubot (bottom). Recall, that every initial state that lies inside the ellipse belongs to the estimated RoA, for which the closed loop dynamics will bring the system back to the upright pose. Hence, a larger (projected) RoA is associated to greater robustness with respect to off-nominal initial states.

One can see on the right-hand side of Fig. 3 that the volume of the estimated RoA of the closed loop dynamics of the top LQR $\mathcal{B}_{\text{est}}$ of $\mathcal{D}_2$ is larger than that of $\mathcal{D}_1$ for the acrobot configuration (1.2 vs. $2.3 \cdot 10^{-4}$), while the converse holds for the pendubot (0.014 vs. 0.037). Note that, even though the RoA of the $\mathcal{D}_2$ acrobot is larger than that of the $\mathcal{D}_1$ pendubot, the estimated RoA of the latter has a larger minor axis (0.014 vs. 0.021), which allows more evenly distributed perturbations around the fixpoint.

B. System Identification

For the system identification, we recorded the data of multiple excitation trajectories with a combined length of about four minutes on both designs of the real double pendulum hardware. We identified the parameters in Table I with a least-squares optimization with a root mean squared error of $\Delta\tau_{rmse} \approx 0.2\,\mathrm{Nm}$ in (2) over all data points for both models. The viscous and coulomb friction parameters of the motors were determined by separate measurements with the individual motors. We set $r_1 = l_1$ after identifying the parameters to list separate values for m_1 and r_1.

C. Robustness Criteria

When transferring controllers from simulation to real hardware many effects that are not present in simulation may influence the behavior. Often it is the case that controllers are tuned in simulation and are capable of high quality

TABLE I: Model parameters

Parameter	Model $\mathcal{M}_1$	Model $\mathcal{M}_2$
mass m [kg]	(0.55, 0.60)	(0.64, 0.56)
length l [m]	(0.3, 0.2)	(0.2, 0.3)
center of mass r [m]	(0.3, 0.183)	(0.2, 0.32)
inertia I [kg m^2]	(0.053, 0.024)	(0.027, 0.054)
motor inertia I_r [kg m^2]	$6.29 \cdot 10^{-5}$	$9.94 \cdot 10^{-5}$
gear ratio g_r	6	6
gravity g [m s^{-2}]	9.81	9.81
viscous friction b [kg m/s]	(0.001, 0.001)	(0.001, 0.001)
coulomb friction c_f [N m]	(0.093, 0.077)	(0.093, 0.077)

performances while in real system experiments they fail to achieve the desired results. This phenomenon is commonly referred to as simulation-reality gap. In order to study the transferability of controllers, we conduct robustness tests in simulation. The robustness tests quantify how well the controllers perform under the following conditions:

1) *Model inaccuracies*: The model parameters, that have been determined with system identification as described in Section III-B, will never be perfectly accurate. To asses inaccuracies in these parameters, we vary the independent model parameters from (3) one at the time in the simulator while using the original model parameters in the controller. The parameters m_1r_1, m_2r_2, m_2, I_1, I_2 are varied between 75% and 125% of their identified values, viscous frictions are varied between -0.1 and 0.1 kg m/s, coulomb friction between -0.2 and 0.2 N m and motor inertia between 0 and 10^{-4} kg m^2.
2) *Measurement noise*: The controllers' outputs depend on the measured system state. In the case of the QDDs, the online velocity measurements are noisy. Hence, it is important for the transferability that a controller can handle at least this amount of noise in the measured data. For testing the robustness, Gaussian noise with standard deviations between 0.0 and 0.5 m/s is added to the velocity measurements. The controllers are tested with and without a low-pass noise filter.
3) *Torque noise*: Not only the measurements are noisy, but also the torque that the controller outputs is not always exactly the desired value. During this test Gaussian noise with standard deviations in the range from 0.0 to 2.0 N m is added to the applied motor torque.
4) *Torque response*: The requested torque of the controller will in general not be constant but change during the execution. The motor, however, is sometimes not able to react immediately to large torque changes and will instead overshoot or undershoot the desired value. This behavior is modelled by applying the torque $\tau = \tau_{t-1} + k_{resp}(\tau_{des} - \tau_{t-1})$ instead of the desired torque τ_{des}. Here, τ_{t-1} is the applied motor torque from the last time step and k_{resp} is the factor which scales the responsiveness. For the tests k_{resp} is varied between 0.1 and 2.0.
5) *Time delay*: When operating on a real system there will always be time delays due to communication and reaction times. For the evaluation, the measurement results are artificially delayed for 0.0 to 0.04 s.

For all above comparisons, the parameters are varied in $N = 21$ steps and for each case it is tested whether the controller is still able to perform a swing-up and reach the final state with an accuracy of $\epsilon = (0.1, 0.1, 0.5, 0.5)$ in the four state dimensions. For the non-deterministic noise tests, ten simulations were conducted for each parameter and the controller has to have at least a 50% success rate to be considered successful. The ranges of the friction parameters b_1, b_2, c_{f1} and c_{f2} extend to negative values because during real system experiments we use friction compensation on both motors. A negative value tests the situation where the friction is overcompensated.

D. Controller Setup

We tested the following controllers for pendubot and acrobot: 1. TVLQR, 2. iLQR MPC (trajectory stabilization), 3. iLQR with Riccati gains, 4. iLQR MPC (free) and 5. Collocated PFL.

For the trajectory stabilization methods the nominal trajectory was computed with iLQR. The trajectory consists of $N = 6000$ time steps with a step size of $\delta t = 0.001$. As we intend to compensate the friction in the motors during the experiments, the friction coefficients were set to 0 for the trajectory optimization. The cost parameters for the trajectory optimization as well as all parameters of the controllers can be found in the supplementary material. The parameters for the LQR and PFL controllers as well as the iLQR trajectory optimization for the acrobot have been obtained with a CMA-ES [18] parameter search with objective to reach the upright position as close as possible. The swing-up trajectory with iLQR computed for the acrobot is visualized in Fig. 4. As the PFL controller is not able to stabilize the double pendulum, it is combined with an LQR controller, which takes over when the cost-to-go falls below a specified value of 15.

E. Robustness Results

We conducted robustness tests for all controllers on both system designs for acrobot and pendubot. All results are listed in Table II, where the listed numbers are the number of successful swing-up attempts out of 21 variations in each category. From the swingup attempts in each category, we computed a success score, which is the percentage of successful swing-up motions of all tested error variations. Fig. 6 visualizes the success scores for both acrobot and pendubot results and for both models in histograms.

As an example, the results for the robustness of the iLQR MPC (trajectory stabilization) controller for the acrobot swing-up with model $\mathcal{M}_1$ are visualized in Fig. 5. In addition to the boolean success criterion, the figure shows the relative

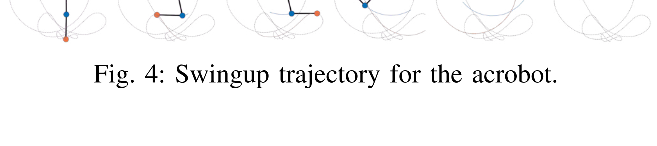

Fig. 4: Swingup trajectory for the acrobot.

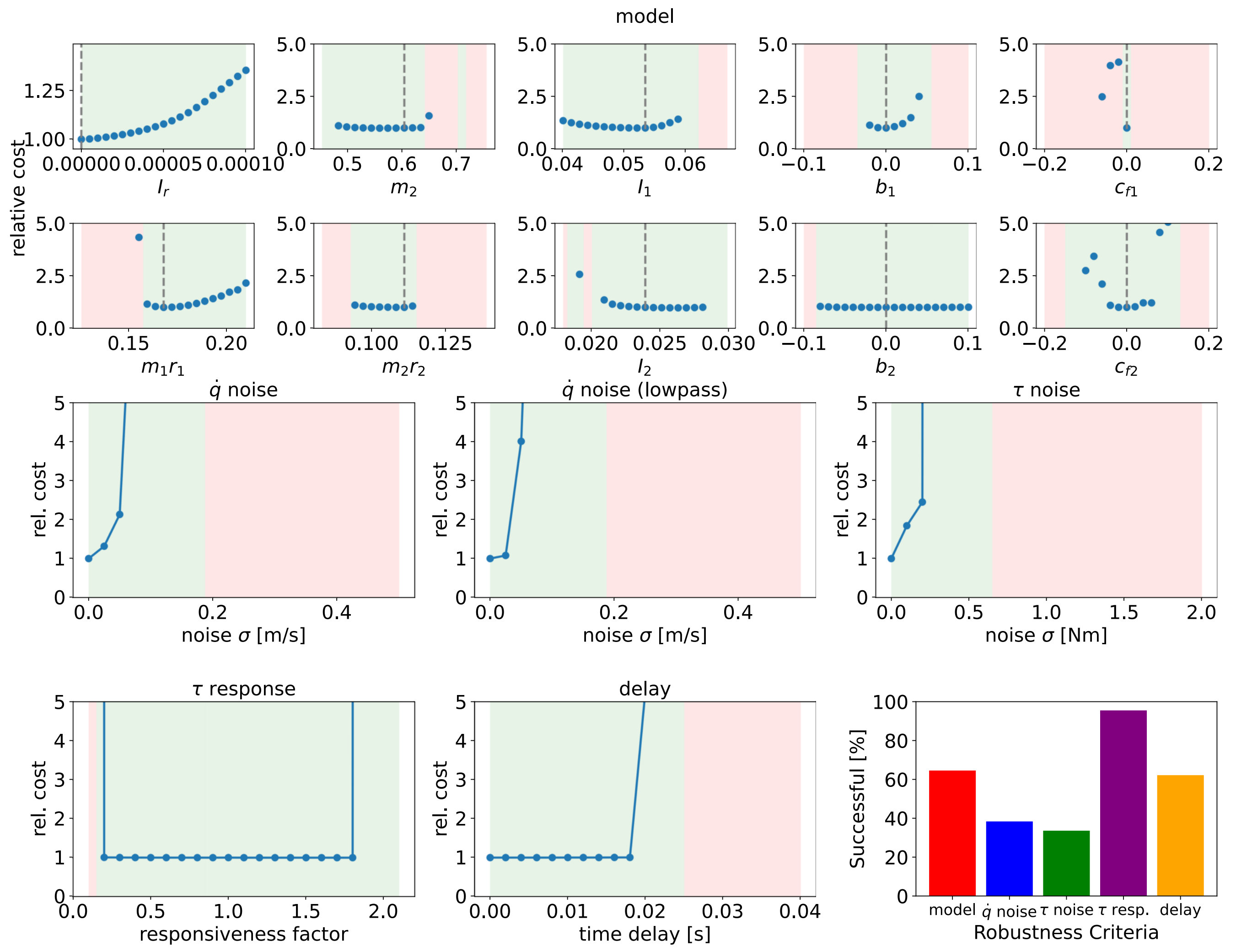

Fig. 5: Robustness to model errors, noise, responsiveness and delay for the iLQR MPC (trajectory stabilization) controller on the acrobot with model $\mathcal{M}_1$ and the trajectory from Fig. 4. The dashed grey lines in the model parameter variations (top two lines) indicate the parameters that the controller uses in its internal model. The model parameters are varied on the x-axis and the y-axis shows the increase in cost relative to the cost with unperturbed model parameters. A green background means that the swing-up was successful while a red background means the swing-up failed. Similarily, the noise responsiveness and delay plots show the const increase and success for varying noise variances, responsiveness factor and delay time. The bottom right shows a histogram of the percentages of successful swingup simulations for each category.

cost increase in the controller's cost function. The first two rows show modelling errors and as expected the cost increases when the controller acts on model parameters that do not match the parameters used for the simulation. It can be observed that the iLQR (stab) controller can deal with changes in the motor inertia I_r, the inertias I_1 and I_2 and the viscous friction b_2 in the second joint. The robustness to changes in m_1r_1, m_2r_2, m_2, b_1 and c_{f2} is a little worse. Most critical are changes in c_{f1}, where small deviations from the correct value prevent a successful swing-up. This is not surprising as the acrobot can not directly compensate for the friction in the first joint and that friction makes dynamic motions at low velocities more difficult. The same controller on the pendubot can deal well with changes in c_{f1} but not so well with changes in c_{f2} (all 21 variations of c_{f1} were successful, see Table II).

When comparing the performance of all controllers, it can be observed that the iLQR (stab) controller achieved the most successful swing-ups on the acrobot configurations ($\mathcal{M}_1$: 191, $\mathcal{M}_2$: 233, out of 315 total attempts) while on the pendubot configurations the TVLQR controller was most successful ($\mathcal{M}_1$: 272, $\mathcal{M}_2$: 244). iLQR (Riccati) receives decent results on the pendubot configurations ($\mathcal{M}_1$: 106, $\mathcal{M}_2$: 145) with the good robustness to noise and responsiveness but less robustness to modelling errors and delay. On the acrobot configuration, iLQR (Riccati) only scores 61 successful swing-ups in both configurations. With at most 20 successful swing-ups across all categories in each configuration, iLQR(free) showed to be very sensitive to all kinds of errors, perturbations or noise. The PFL controller showed little robustness on the $\mathcal{M}_1$ acrobot configuration but performed well in all other configurations (Acrobot: $\mathcal{M}_1$: 26,

	m_1r_1	m_2r_2	m_2	I_1	I_2	I_r	b_1	b_2	c_{f1}	c_{f2}	$\dot{q}_{noise}$	$\dot{q}_{noise}$ (filt.)	τ_{noise}	τ_{resp}	delay	total
$\mathcal{M}_1$ Acrobot																382
TVLQR	6	6	2	2	1	5	1	2	1	2	6	5	**18**	19	8	84
iLQR (stab)	**13**	**8**	**14**	**17**	**19**	**21**	**9**	**19**	1	**14**	**8**	**8**	7	**20**	**13**	**191**
iLQR (Riccati)	1	3	1	1	1	4	1	2	1	3	6	5	10	19	3	61
iLQR (free)	1	1	1	1	1	1	2	1	**3**	1	1	1	1	1	3	20
PFL	3	1	1	2	2	2	1	1	1	2	1	1	1	2	5	26
$\mathcal{M}_2$ Acrobot																634
TVLQR	11	1	1	12	1	4	1	8	3	13	8	8	**21**	**21**	7	120
iLQR (stab)	**15**	**10**	**16**	**21**	16	**21**	**14**	**21**	**9**	**18**	12	11	14	19	**16**	**233**
iLQR (Riccati)	1	1	1	1	1	1	1	2	1	3	8	8	13	17	2	61
iLQR (free)	1	1	1	1	1	2	1	1	1	1	1	1	1	1	3	18
PFL	14	9	14	19	**17**	19	10	11	1	9	**16**	**15**	**21**	20	7	202
$\mathcal{M}_1$ Pendubot																861
TVLQR	**21**	**18**	**18**	**21**	**21**	18	**21**	7	**21**	5	**21**	**21**	**21**	**21**	**17**	**272**
iLQR (stab)	**21**	15	16	**21**	17	14	**21**	7	**21**	6	8	8	15	20	15	225
iLQR (Riccati)	4	2	2	5	2	2	1	1	2	1	**21**	**21**	14	**21**	7	106
iLQR (free)	1	1	1	1	2	1	1	1	1	2	1	1	1	1	3	19
PFL	19	16	16	18	16	**20**	19	3	**21**	**11**	16	15	19	19	11	239
$\mathcal{M}_2$ Pendubot																827
TVLQR	19	**18**	**17**	**21**	**17**	**17**	17	3	16	1	**21**	**21**	**21**	20	**15**	**244**
iLQR (stab)	**21**	15	16	**21**	**17**	16	**21**	**10**	**21**	**12**	4	4	5	15	11	209
iLQR (Riccati)	16	3	2	14	3	3	3	1	5	3	**21**	**21**	**21**	**21**	8	145
iLQR (free)	1	1	1	1	1	1	1	1	1	1	1	1	1	1	3	17
PFL	18	12	12	**21**	14	15	14	2	15	8	13	14	21	19	14	212

TABLE II: Results of all robustness tests which were conducted in simulation. Listed are the number of successful swing-ups out of 21 variations of the quantity in the header.

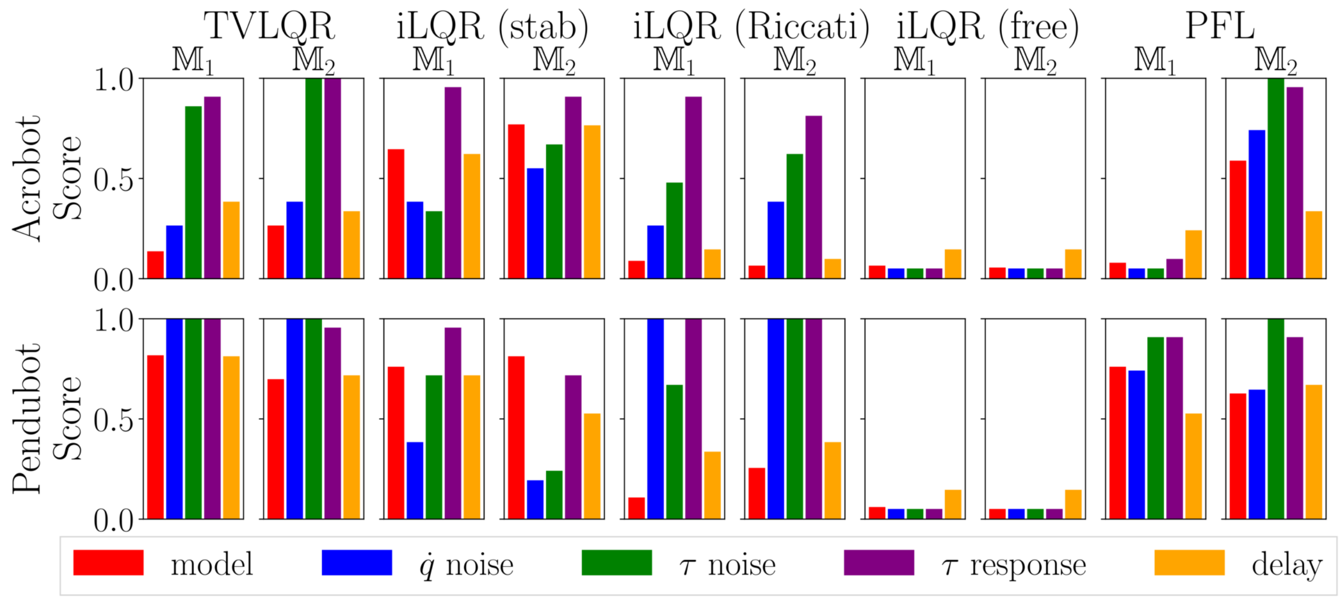

Fig. 6: Success scores of the robustness tests for all controllers applied to acrobot and pendubot.

$\mathcal{M}_2$: 202, Pendubot: $\mathcal{M}_1$: 239, $\mathcal{M}_2$: 212).

The robustness results can also be used to quantify the difficulty of the swing-up task on the different configurations. Summing up all scores on the acrobot configurations yields 382 successful swing-ups on model $\mathcal{M}_1$ and 634 on model $\mathcal{M}_2$, clearly indicating that the swing-up task on the acrobot with the longer second link ($\mathcal{M}_2$) is easier than when the link lengths are reversed ($\mathcal{M}_1$). This is consistent with the region of attraction analysis that was used during the system design in section IV-A. In the case of the pendubot, there are 861 successful swing-ups on the $\mathcal{M}_1$ model and 827 on the $\mathcal{M}_2$ model. This confirms that for the pendubot the $\mathcal{M}_1$ model poses the easier task and that the difference in difficulty is less significant as it was the case when comparing the region of attractions of the pendubot LQR controller.

V. Experiments

1) Setup: The QDDs from T-motors pose some challenges on the control algorithms due to presence of noise in velocity measurements with standard deviations of $\sigma_{\dot{q}} = 0.05\,\frac{\text{rad}}{\text{s}}$

and torque noise with $\sigma_\tau = 0.05\,\mathrm{Nm}$. The torque response factor k_{resp} ranges between 0.4 and 0.9. The operating delay lies between 0.005 s and 0.01 s. To achieve more dynamical motions, we used friction compensation in both motors for the acrobot and in the passive motor for the pendubot.

2) Acrobot Results: For the acrobot swing-up, we tested the TVLQR controller to stabilize the iLQR trajectory on model $\mathcal{M}_2$. The results are displayed in Figure 7(a), where the colored dashed lines show the nominal trajectory that the TVLQR controller is supposed to stabilize and the solid lines show the actual measured positions, velocities and torques. The controller tracks the trajectory well except for the final part, which is the most challenging as the high velocities in this phase cause vibrations in the system. Due to the imperfect final phase, we tested the stabilization with LQR in a separate experiment. The LQR controller is able to stabilize the acrobot and the controller is able to recover from relatively large state deviations as pictured in Fig. 7(c).

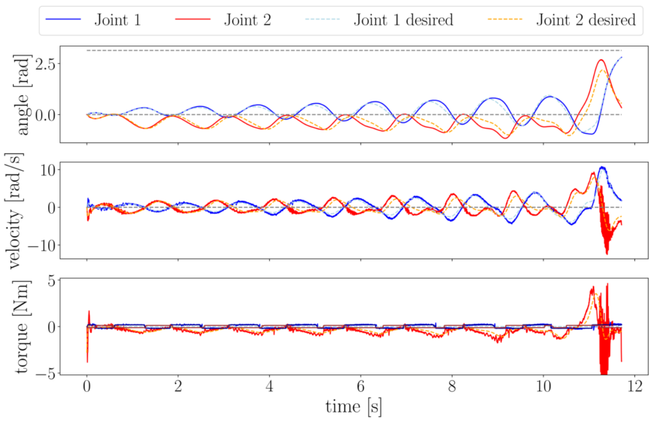

(a) Recorded data of acrobot swing-up with TVLQR.

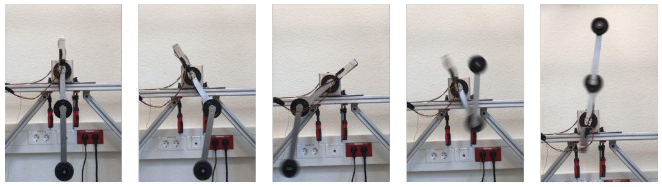

(b) Pictures of acrobot swing-up with TVLQR.

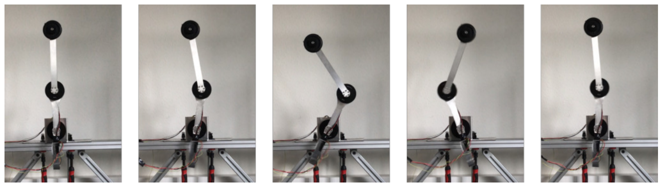

(c) Pictures of acrobot stabilization with LQR.

Fig. 7: Acrobot swing-up and stabilization on the real system with TVLQR and LQR (separate experiments).

3) Pendubot Results: Based on the robustness tests in Section IV, the most robust controller for the pendubot with model $\mathcal{M}_1$ is the TVLQR controller. For the experiment, we combined the TVLQR controller with an LQR controller for the stabilization after the swing-up. The TVLQR controller is indeed able to perform a successful swing-up on the real system and the LQR controller is able to stabilize the unstable fixpoint afterwards. The data recorded during the experiment can be seen in Fig. 8(a). At $t \approx 4.5\,\mathrm{s}$, the control switches from the TVLQR trajectory stabilization to the LQR fix point stabilization. The pendulum follows the position and velocity of the desired trajectory closely. The torque that is necessary for the tracking deviates noticeably from the nominal torque, especially at the peaks and during the final phase of the swing-up. During the LQR stabilization phase the control output switches between minimum and maximum torque with a high frequency. Attempts to tune the LQR parameters by hand to avoid this behavior were not successful. However, the LQR stabilization is stable and can also be perturbed with a stick. The pendulum only drops once the controller is switched off.

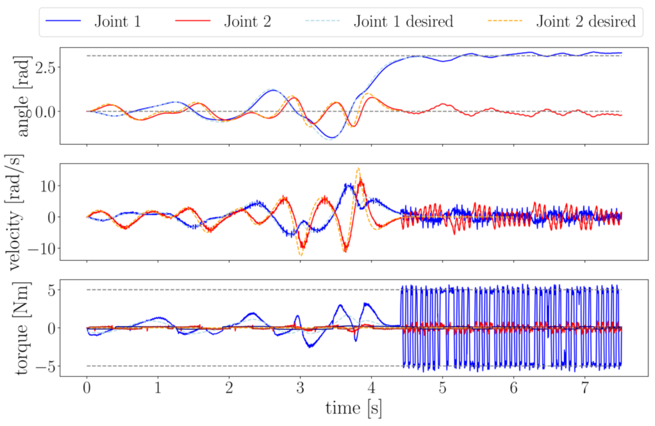

(a) Recorded data of pendubot swing-up (TVLQR) and stabilization (LQR).

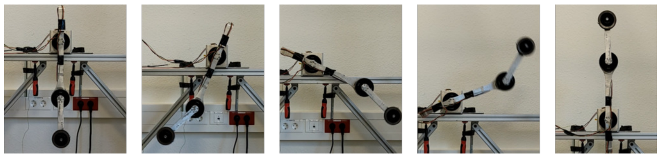

(b) Pictures of pendubot swing-up.

Fig. 8: Pendubot swing-up on the real system. The switch from TVLQR to LQR stabilization happens at $t \approx 4.5\,\mathrm{s}$

.

VI. Conclusion

We introduced a canonical hardware platform which allows the comparison of the performance of different control algorithms. The double pendulum can be operated either as a pendubot or as an acrobot without changes in the hardware. The double pendulum design can be changed with different link lengths and a different attached mass at the tip which creates systems with different difficulty for the controller. In this paper, we evaluated the performance of the controllers: LQR, TVLQR, PFL and three versions based on iLQR. We tested their robustness to model inaccuracies, noise, motor response and delay and demonstrated a successful pendubot swing-up with TVLQR on the real hardware. The necessary hardware components are inexpensive and all software from the drivers to the operating software and controllers is open source. The double pendulum is integrated in RealAIGym [19] along with other canonical systems. The transparency of this project has two major advantages for the robotics research community. First, it enables reproducibility of experimental results, which is of major importance for sustainable scientific research. Second, the availability and openness allows students and newcomers in the field to study dynamic control at any level without boundaries set by high costs, licences or closed software.

VII. Reproducibility

The entire platform is designed to be replicated for reproducing and improving on existing results. Two key aspects are that the hardware is inexpensive and that all software is openly available[8], including all scripts and data which were used to obtain the results from this paper. Additionally, software is archived at Zenodo[9] and the simulations from this paper are uploaded to Code Ocean[10] to be run online without the need for a local installation. The github repository also contains all necessary files for rebuilding the double pendulum test bench such as the mechanical design, CAD models, bill of materials, etc. Instructions for the assembly of the hardware setup with step by step pictures can be found in the same repository as well as in the supplementary materials for this paper. The supplementary material also contains more detailed descriptions of the controllers including pseudocode, more details for operating the hardware and more benchmark results.

This work complies with the Good Experimental Methodology (GEM) Guidelines [20]. This paper introduces an open source and low-cost test bench and contains experiments conducted in simulation and on real hardware (Q1). We lay out the assumptions and research questions in sections III and IV (Q2). In section IV, we also explain the evaluation criteria (Q3) and how they are measured (Q4). The robustness criteria quantify the sensitivity of the controllers and allow for a comparison of the difficulty of the swing up task on the acrobot and pendubot platforms (Q5). We published all relevant information and data for reproducing our work (Q6) and thoroughly reported methods, parameters and results to give a realistic picture of our results (Q7) and draw conclusions in section VI (Q8). A summarizing table of the GEM guidelines and the compliance of this paper can be found in the supplementary material.

References

[1] B. Katz, J. Di Carlo, and S. Kim, "Mini cheetah: A platform for pushing the limits of dynamic quadruped control," in *2019 International Conference on Robotics and Automation (ICRA)*. IEEE, 2019, pp. 6295–6301.

[2] G. Brockman, V. Cheung, L. Pettersson, J. Schneider, J. Schulman, J. Tang, and W. Zaremba, "Openai gym," *arXiv preprint arXiv:1606.01540*, 2016.

[3] A. Raffin, A. Hill, A. Gleave, A. Kanervisto, M. Ernestus, and N. Dormann, "Stable-baselines3: Reliable reinforcement learning implementations," *Journal of Machine Learning Research*, vol. 22, no. 268, pp. 1–8, 2021. [Online]. Available: http://jmlr.org/papers/v22/20-1364.html

[4] J. Hauser and R. M. Murray, "Nonlinear controllers for non-integrable systems: The Acrobot example," in *Proceedings of the American Control Conference*, no. 1, 1990, pp. 669–671.

[5] S. Bortoff, "Advanced nonlinear robotic control using digital signal processing," *IEEE Transactions on Industrial Electronics*, vol. 41, no. 1, pp. 32–39, 1994.

[6] M. W. Spong, "The swing up control problem for the Acrobot," *IEEE Control Systems*, vol. 15, no. 1, pp. 49–55, feb 1995.

[7] N. A. Andersen, L. Skovgaard, and O. Ravn, "Control of an under actuated unstable nonlinear object," in *Experimental Robotics VII*. Berlin, Heidelberg: Springer Berlin Heidelberg, 2007, pp. 481–490.

[8] X. Xin and T. Yamasaki, "Energy-Based Swing-Up Control for a Remotely Driven Acrobot: Theoretical and Experimental Results," *IEEE Transactions on Control Systems Technology*, vol. 20, no. 4, pp. 1048–1056, jul 2012.

[9] A. Majumdar, A. A. Ahmadi, and R. Tedrake, "Control design along trajectories with sums of squares programming," in *2013 IEEE International Conference on Robotics and Automation*. IEEE, may 2013, pp. 4054–4061.

[10] K. Van Heerden, Y. Fujimoto, and A. Kawamura, "A combination of particle swarm optimization and model predictive control on graphics hardware for real-time trajectory planning of the under-actuated nonlinear Acrobot," in *2014 IEEE 13th International Workshop on Advanced Motion Control (AMC)*. IEEE, mar 2014, pp. 464–469.

[11] T. Horibe and N. Sakamoto, "Nonlinear Optimal Control for Swing Up and Stabilization of the Acrobot via Stable Manifold Approach: Theory and Experiment," *IEEE Transactions on Control Systems Technology*, vol. 27, no. 6, pp. 2374–2387, nov 2019.

[12] H. G. González-Hernández, J. Alvarez, and J. Alvarez-Gallegos, "Experimental analysis and control of a chaotic pendubot," *International Journal of Robotics Research*, vol. 23, no. 9, pp. 891–901, 2004.

[13] F. B. Mathis, R. Jafari, and R. Mukherjee, "Impulsive actuation in robot manipulators: Experimental verification of pendubot swing-up," *IEEE/ASME Transactions on Mechatronics*, vol. 19, no. 4, pp. 1469–1474, 2014.

[14] R. Ng, Y. Tang, H. Lin, X. Chu, and K. W. S. Au, "Development of a Portable Hybrid Pendubot-Acrobot Robotic Platform for On and Off-Campus Teaching and Learning," in *2021 American Control Conference (ACC)*, vol. 2021-May. IEEE, may 2021, pp. 98–105.

[15] L. Weiwei and E. Todorov, "Iterative Linear Quadratic Regulator Design for Nonlinear Biological Movement Systems." *International Conference on Informatics in Control, Automation and Robotics*, pp. 222–229, 2004.

[16] S. Kleff, A. Meduri, R. Budhiraja, N. Mansard, and L. Righetti, "High-frequency nonlinear model predictive control of a manipulator," in *2021 IEEE International Conference on Robotics and Automation (ICRA)*. IEEE, 2021, pp. 7330–7336.

[17] L. Maywald, F. Wiebe, S. Kumar, M. Javadi, and F. Kirchner, "Co-optimization of acrobot design and controller for increased certifiable stability," in *IEEE/RSJ International Conference on Intelligent Robots and Systems (IROS-2022)*, 10 2022.

[18] N. Hansen, *The CMA Evolution Strategy: A Comparing Review*. Berlin, Heidelberg: Springer Berlin Heidelberg, 2006, pp. 75–102. [Online]. Available: https://doi.org/10.1007/3-540-32494-1_4

[19] F. Wiebe, S. Vyas, L. J. Maywald, S. Kumar, and F. Kirchner, "RealAIGym: Education and Research Platform for Studying Athletic Intelligence," in *Proceedings of Robotics Science and Systems Workshop Mind the Gap: Opportunities and Challenges in the Transition Between Research and Industry*, New York, July 2022.

[20] F. Bonsignoriom, J. Hallam, and A. P. del Pobil, "Special Interest Group GOOD EXPERIMENTAL METHODOLOGY, GEM Guidelines," http://www.heronrobots.com/EuronGEMSig/downloads/GemSigGuidelinesBeta.pdf, accessed: 11-04-2023.

[8] https://github.com/dfki-ric-underactuated-lab/double_pendulum

[9] https://zenodo.org/record/7529896

[10] https://codeocean.com/capsule/2798174/tree